GEOMETRICALLY NONLINEAR BENDING MESH-FREE ANALYSIS OF FUNCTIONALLY GRADED POROUS SANDWICH BEAM

Tran Quang Hung[1], Tran Minh Tu[2], Do Minh Duc[1]*

[1]The University of Danang - University of Science and Technology, Danang, Vietnam
[2]Hanoi University of Civil Engineering, Hanoi, Vietnam

*Corresponding author: ducdhbk@gmail.com

(Received: March 20, 2023; Revised: May 9, 2023; Accepted: May 25, 2023)

Abstract - In this work, geometrically nonlinear static bending analysis of sandwich beams with a porous core and two skins made of functionally graded materials using a mesh-free method is presented. The material types of the core and face sheets of the beam are chosen so that the material continuity between the layers is guaranteed. The nonlinear governing equation including geometric nonlinearity is established via the principle of virtual work. This equation is discretized into a system of algebraic equations by the mesh-free approach, which is based on the C^1 point interpolation method and polynomial basis functions, and then solved by the direct iterative method. The convergence of the mesh-free method is tested to determine the sufficient mesh level for the analysis. Comparative and comprehensive studies are performed to investigate both the correctness and the influences of several important parameters and boundary conditions on the linear and nonlinear deflections of the beam.

Key words - Geometrically nonlinear bending; functionally graded materials; porous material; porous sandwich beam; mesh-free analysis

1. Introduction

Sandwich structures composed of a porous core and two functionally graded material (FGM) skins, shortened here as PFGM sandwich structures for convenience, offer many excellent features. While the FGM skins have high stiffness, and good ability of thermal, corrosion, and weather resistance, the porous material core is lightweight and efficient for thermal and sound insulation as well as for energy absorption. Furthermore, by tailoring the materials of the skins and the core appropriately, physical properties can be smooth in the whole domain of the structures. Thus, the stress concentration, which may lead to delamination, at the interface layers can be avoided. To enhance the efficiency of application in reality, studying to explore the mechanical behavior of these structures becomes an essential task. Many reports related to this topic by authors are now available in the literature. For example, Mu and Zhao [1] examined the first natural frequency of PFGM sandwich beams by extended Galerkin method. Wang et al. [2] focused on the time history response of PFGM sandwich beams excited by a non-uniformly distributed moving mass employing Chebyshev–Ritz approximation. Chinh et al. [3] presented the static bending of the PFGM sandwich beam by Reddy's shear deformation beam model. Hung and Truong [4] performed the free vibration response of PFGM sandwich beams resting on the Winkler foundation using various beam models. Using the Ritz technique, Hung et al. [5] dealt with the thermo-electrical free vibration of PFGM sandwich beams inserted into two piezoelectric layers and resting on a two-parameter elastic foundation. Adopting Navier's solution, Hung et al. [6] investigated the static behavior of a PFGM sandwich beam considering the influence of the liquid phase in the porous core. Derikvand et al. [7] studied the buckling of PFGM sandwich beams by the differential transform method associated with the framework of third-order shear deformation beam theory. Duc et al. [8] analyzed the nonlinear buckling and post-buckling of PFGM sandwich stiffened truncated conical shells lying on a two-parameter elastic foundation. Nguyen and co-workers [9] presented the static flexural and free vibration response of a PFGM sandwich plate with graphene platelets (GPLs) reinforcement by isogeometric analysis.

In mechanical modeling, structural analysis with formulations established by the assumption of ignoring the deformation (not updated with the deformation), also called geometrically linear analysis, is simple and computationally inexpensive. However, for slender structures/structures under heavy load, the deformation is significant; thus, this assumption does not reflect their realistic behavior and may lead to serious design errors. To overcome the limitation, the geometrically nonlinear analysis considering the deformation effect becomes necessary. Beams are primary elements used for structural constructions. Modeling the mechanical behavior of beams with the consideration of geometrical nonlinear effects has been studied by several authors. For example, Lin et al. [10] simulated the geometrically nonlinear bending of FGM beams with variable thickness by using a meshless Smoothed Hydrodynamic Particle method. Utilizing Chebyshev–Ritz method, Wang et al. [11] reported the geometrically nonlinear bending behavior of sandwich beams consisting of composite skins with agglomerated GPL reinforcement and a metal foam core. Jedari Salami [12] investigated the geometrically nonlinear bending of sandwich beams with functionally graded graphene platelet-reinforced composite (GPLRC) skins and polyurethane foam core using the Ritz method. Srikarun et al. [13] focused on the linear and nonlinear bending of sandwich beams with isotropic skins and a porous core under various types of distributed load by utilizing the Gram-Schmidt-Ritz method. Feng et al. [14] investigated the geometrically nonlinear behavior of composite beams reinforced with GPLs employing Ritz approximation. Li et al. [15] investigated the geometrically nonlinear bending response of two-dimensional FGM beams using the generalized differential quadrature method. Reddy et al.

[16] developed finite element models for FGM microbeams including the von Kármán non-linearity. Zhang [17] presented a model for geometrically nonlinear analysis of FGM beams in the thermal environment by the physical neutral concept and the Ritz method.

To the best of the authors' knowledge, although there have been several studies on the nonlinear bending behavior of sandwich beams, more in-depth studies are still needed for new structural elements. Therefore, in this paper, for the first time, the nonlinear bending analysis of sandwich beams consisting of FGM face sheets and anFG porous core is conducted. The material's continuity between the layers is guaranteed by choosing appropriate skins and core materials. Based on Reddy's third-order beam theory and geometrical nonlinearity, the nonlinear governing equations are derived from the virtual work principle incorporated. The mesh-free approach, using C^1 point interpolation method and polynomial basis functions, is adopted to discretize the governing equation into algebraic equations and then solved by the direct iterative method. The convergence is conducted to determine the sufficient mesh level for the analysis. The correctness of the current study is validated by comparing the study results with those of other publications in the literature. A parametric study is also conducted to examine in detail the effects of the power-law index, porosity coefficient, core-to-skin thickness ratio, and edge conditions on the linear and nonlinear deflections of the beam.

2. Basic formulations

2.1. PFGM sandwich beam and material properties

Consider a PFGM sandwich beam of dimensions $L\times b\times h$ as illustrated in Figure 1. The thicknesses of the skins and the porous core are denoted as h_f and h_c, respectively ($h = h_c + 2h_f$). The z-axis is in the vertically upward direction, and the x-axis belongs to the mid-plane. The two similar skins are made of FGM which is a mixture of ceramic and metal. The core is constructed of a metal foam, which is a type of porous material. The beam is subjected to a transverse load with an amplitude of $q_o(x)$ on the top surface.

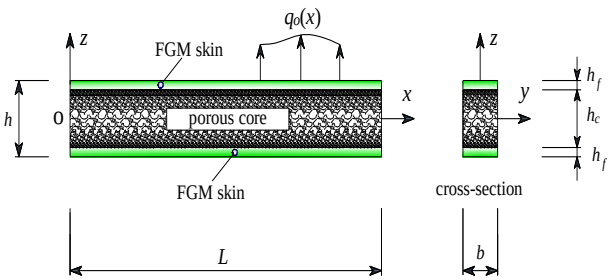

***Figure 1**. Configuration and geometrical parameters of PFGM sandwich beam*

There are many mathematical models proposed for designing the variations of mechanical properties of FGM and metal foam. The power law and cosine rule variations are widely used for the former and the latter, respectively. Based on these variations, the effective Young's modulus (E) of the two FGM skins and the core is assumed to change along the thickness of the beam as follows [2, 3]:

$$\begin{cases} E(z) = (E_m - E_c)\left[(0.5h - z)/h_f\right]^k + E_c, & \text{(top skin)} \\ E(z) = E_m\left[1 - e_o\cos(\pi z/h_c)\right], & \text{(porous core)} \\ E(z) = (E_m - E_c)\left[(0.5h + z)/h_f\right]^k + E_c, & \text{(bottom skin)} \end{cases} \quad (1)$$

in which E_m and E_c are Young's moduli of two primary materials composing FGM of the skins; the pure material of metal foam (having no pores) is the same as the metal constituent of the FGM skins; k is the power-law index ($0 \le k$); e_o is the porosity coefficient ($0 \le e_o < 1$). It is evident from Eq. (1) that Young's modulus E varies continuously in the whole domain of the beam. Poisson's ratio (ν) is assumed to be constant for each layer, and shear modulus can be determined via the relation $G(z) = E(z)/(2+2\nu)$.

2.2. Displacement, strain and stress fields

In this work, based on the framework of third-order beam theory (TOBT), the components $u(x, z)$, $w(x, z)$ of the displacement field, which are, respectively, corresponding to the x- and z-directions, can be expressed as

$$\begin{cases} \mathbf{d} = \begin{Bmatrix} u \\ w \end{Bmatrix} = \underbrace{\begin{bmatrix} 1 & 0 & -z & \kappa(z) \\ 0 & 1 & 0 & 0 \end{bmatrix}}_{\mathbf{\Theta}_1}\mathbf{A}_1 = \mathbf{\Theta}_1\mathbf{A}_1 \\ \kappa(z) = z - \dfrac{4}{3}\dfrac{z^3}{h^2} \\ \mathbf{A}_1^{\mathrm{T}} = \left\{ u_o(x) \quad w_o(x) \quad \dfrac{\partial w_o(x)}{\partial x} \quad \theta_o(x) \right\} \end{cases} \quad (2)$$

Where, u_o, w_o, and θ_o are the axial displacement, transverse displacement, and the shear strain on the mid-plane (i.e., $z = 0$), respectively. They are three primary variable functions of the problem which need determining.

The strain field based on the von Kármán geometric nonlinearity can be given by

$$\boldsymbol{\varepsilon} = \begin{Bmatrix} \varepsilon_x \\ \gamma_{xz} \end{Bmatrix} = \underbrace{\begin{bmatrix} 1 & -z & \kappa(z) & 0 \\ 0 & 0 & 0 & \dfrac{\partial\kappa(z)}{\partial z} \end{bmatrix}}_{\mathbf{\Theta}_2}\mathbf{A}_2 + \ldots + \begin{bmatrix} 1/2 \\ 0 \end{bmatrix}\left(\frac{\partial w_o}{\partial x}\right)^2 = \mathbf{\Theta}_2\mathbf{A}_2 + \begin{bmatrix} 1/2 \\ 0 \end{bmatrix}\left(\frac{\partial w_o}{\partial x}\right)^2 \quad (3)$$

$$\mathbf{A}_2^{\mathrm{T}} = \left\{ \frac{\partial u_o}{\partial x} \quad \frac{\partial^2 w_o}{\partial x^2} \quad \frac{\partial \theta_o}{\partial x} \quad \theta_o \right\} \quad (4)$$

The stress-strain relationships obey Hook's law and can be presented in a compact form as

$$\boldsymbol{\sigma} = \begin{Bmatrix} \sigma_x \\ \tau_{xz} \end{Bmatrix} = \underbrace{\begin{bmatrix} E(z) & 0 \\ 0 & G(z) \end{bmatrix}}_{\mathbf{E}_d}\boldsymbol{\varepsilon} = \mathbf{E}_d\boldsymbol{\varepsilon} \quad (5)$$

2.3. Energy expressions

The variation of internal energy (δW) of the PFGM sandwich beam can be determined as follows:

$$\delta W = \int_V \delta\boldsymbol{\varepsilon}^{\mathrm{T}}\boldsymbol{\sigma}dV = \int_V \delta\boldsymbol{\varepsilon}^{\mathrm{T}}\mathbf{E}_d\boldsymbol{\varepsilon}dV \tag{6}$$

Next, plugging the strains from Eq. (3) into Eq. (6), the variation of internal energy can be described by

$$\begin{aligned}\delta W = &\int_0^L \delta\mathbf{A}_2^{\mathrm{T}}\mathbf{D}_{E1}\mathbf{A}_2 dx + \int_0^L \frac{\partial\delta w_o^{\mathrm{T}}}{\partial x}\mathbf{D}_{E2}\mathbf{A}_2 dx + \\ &+ \int_0^L \frac{\partial\delta w_o^{\mathrm{T}}}{\partial x}\mathbf{D}_{E3}\frac{\partial w_o}{\partial x}dx + \int_0^L \delta\mathbf{A}_2^{\mathrm{T}}\mathbf{D}_{E4}\frac{\partial w_o}{\partial x}dx\end{aligned} \tag{7}$$

Where, $\mathbf{D}_{E1}$, $\mathbf{D}_{E2}$, $\mathbf{D}_{E3}$ and $\mathbf{D}_{E4}$ are the matrices of stiffness coefficients which are defined as

$$\begin{cases}\mathbf{D}_{E1} = b\displaystyle\int_{-0.5h}^{0.5h}\boldsymbol{\Theta}_2^{\mathrm{T}}\mathbf{E}_d\boldsymbol{\Theta}_2 dz; \\ \mathbf{D}_{E2} = b\displaystyle\int_{-0.5h}^{0.5h}\frac{\partial w_o^{\mathrm{T}}}{\partial x}\{1 \quad 0\}\mathbf{E}_d\boldsymbol{\Theta}_2 dz; \\ \mathbf{D}_{E3} = b\displaystyle\int_{-0.5h}^{0.5h}\{1 \quad 0\}\mathbf{E}_d\begin{Bmatrix}1/2\\0\end{Bmatrix}\left(\frac{\partial w_o}{\partial x}\right)^2 dz; \\ \mathbf{D}_{E4} = b\displaystyle\int_{-0.5h}^{0.5h}\boldsymbol{\Theta}_2^{\mathrm{T}}\mathbf{E}_d\begin{Bmatrix}1/2\\0\end{Bmatrix}\frac{\partial w_o}{\partial x}dz\end{cases} \tag{8}$$

Eq. (8) shows that the stiffness coefficients in the matrices $\mathbf{D}_{E2}$, $\mathbf{D}_{E3}$ and $\mathbf{D}_{E4}$ depend on the transverse displacement $w_o(x)$ of the beam, except for those in $\mathbf{D}_{E1}$.

The variation of external work (δS) done by the transverse load $q_o(x)$ can be expressed by

$$\delta S = -\int_0^L q_o\delta w_o(x)dx \tag{9}$$

In the mechanical analysis, the principle of virtual work can be employed to derive the equilibrium equation of the system. It can be stated as the following formula

$$\delta W + \delta S = 0 \tag{10}$$

2.4. Mesh-free approach

Various analytical and numerical methods can be used to find out the primary variable functions of the problem. This study employs the mesh-free method developed by Hung et al. [18] to obtain approximate solutions.

2.4.1. Approximation of displacement fields

The variable functions need approximating through their function values at nodes, also called the nodal values, in the problem domain. This means that the discretized nodal values become the alternative unknowns. In what follows, the detailed procedure of the approximation is presented.

Consider an influence domain Ω_s which is a sub-domain of the problem domain Ω. The domain Ω_s is represented by N arbitrarily distributed nodes along the x-axis. In Ω_s, an arbitrary function $\hat{h}_o(x)$ can be approximated using C^1 Hermite interpolation as

$$\hat{h}_o(x) = \sum_{i=1}^{2N}\chi_i\,\xi_i = \boldsymbol{\chi}^{\mathrm{T}}\boldsymbol{\xi} \tag{11}$$

Where, $\boldsymbol{\xi}$ and $\boldsymbol{\chi}$ denote the vectors of coefficients and polynomial basis, respectively.

$$\boldsymbol{\chi}^{\mathrm{T}}(x) = \left\{1 \;\; x \;\; x^2 \;\; \ldots \;\; x^{2N-1}\right\} \tag{12}$$

$$\boldsymbol{\xi} = \left\{\xi_1 \;\; \xi_2 \;\; \ldots \;\; \xi_{2N}\right\}^{\mathrm{T}} \tag{13}$$

To determine the unknown coefficients in the vector $\boldsymbol{\xi}$, function $\hat{h}_o(x)$ of Eq. (11) is enforced to pass through the nodal values at nodes in the influence domain. For example, the enforcement for the node m-th at the coordinates $x = x_m$ can be written as

$$\mathbf{q}_m = \begin{Bmatrix}\eta_{om}\\ \varphi_{om}\end{Bmatrix} = \begin{Bmatrix}\displaystyle\sum_{i=1}^{2N}\chi_i(x_m)\xi_i \\ \displaystyle\sum_{i=1}^{2N}\frac{\partial\chi_i(x_m)}{\partial x}\xi_i\end{Bmatrix} = \begin{Bmatrix}\boldsymbol{\chi}^{\mathrm{T}}(x_m)\boldsymbol{\xi} \\ \dfrac{\partial\boldsymbol{\chi}^{\mathrm{T}}(x_m)}{\partial x}\boldsymbol{\xi}\end{Bmatrix} \tag{14}$$

in which η_{om} and φ_{om} represent the function values (nodal values) of $\hat{h}_o(x)$ and $\partial\hat{h}_o(x)/\partial x$ at $x = x_m$, respectively.

For $m = 1, \ldots, N$, Eq. (14) can then be described in the compact form as follows

$$\mathbf{q} = \mathbf{P}_Q\boldsymbol{\xi} \tag{15}$$

Where, $\mathbf{P}_Q$ is the moment matrix of size ($2N \times 2N$) that is evaluated by

$$\mathbf{P}_Q = \begin{Bmatrix}\boldsymbol{\chi}^{\mathrm{T}}(x_1) & \dfrac{\partial\boldsymbol{\chi}^{\mathrm{T}}(x_1)}{\partial x} & \boldsymbol{\chi}^{\mathrm{T}}(x_2) & \dfrac{\partial\boldsymbol{\chi}^{\mathrm{T}}(x_2)}{\partial x} & \ldots \\ & \ldots. & \boldsymbol{\chi}^{\mathrm{T}}(x_N) & \dfrac{\partial\boldsymbol{\chi}^{\mathrm{T}}(x_N)}{\partial x} & \end{Bmatrix}^{\mathrm{T}} \tag{16}$$

and vector $\mathbf{q}$ contains the nodal values in the domain Ω_s:

$$\mathbf{q} = \left\{\eta_{o1} \;\; \varphi_{o1} \;\; \eta_{o2} \;\; \varphi_{o2} \;\; \ldots \;\; \eta_{oN} \;\; \varphi_{oN}\right\}^{\mathrm{T}} \tag{17}$$

From Eq. (15), vector $\boldsymbol{\xi}$ is determined by the inverse of matrix:

$$\boldsymbol{\xi} = \mathbf{P}_Q^{-1}\mathbf{q} \tag{18}$$

The approximate function $\hat{h}_o(x)$ is obtained by substituting back vector $\boldsymbol{\xi}$ into Eq. (10):

$$\hat{h}_o(x) = \boldsymbol{\chi}^{\mathrm{T}}\boldsymbol{\xi} = \underbrace{\boldsymbol{\chi}^{\mathrm{T}}\mathbf{P}_Q^{-1}}_{\boldsymbol{\psi}(x)}\mathbf{q} = \boldsymbol{\psi}(x)\mathbf{q} \tag{19}$$

Where, $\boldsymbol{\psi}(x)$ is called the vector of shape functions. This vector is defined by

$$\boldsymbol{\psi}(x) = \begin{Bmatrix}\psi^{(1)}(x) & \psi_\varphi^{(1)}(x) & \psi^{(2)}(x) & \\ \psi_\varphi^{(2)}(x) & \ldots & \psi^{(N)}(x) & \psi_\varphi^{(N)}(x)\end{Bmatrix} = \boldsymbol{\chi}^{\mathrm{T}}\mathbf{P}_Q^{-1} \tag{20}$$

The vector of shape functions $\boldsymbol{\psi}(x)$ that is established

for $\hat{h}_o(x)$ is then employed to approximate all the primary unknowns of the problem, i.e., $u_o(x)$, $w_o(x)$, and $\theta_o(x)$.

Note that the nodal values of different functions at the same node are different.

2.4.2. Discrete form

According to the mesh-free method, the domain of the PFGM beam is discretized into a set of sub-domains Ω_c called background cells. Ω_c can be independent of the influence domains. Supposing that Ω_c belongs to the influence domain Ω_s. Hence, the unknown functions of the problem in Ω_c, i.e., $u_o(x)$, $w_o(x)$, and $\theta_o(x)$ can be approximated through their nodal values by using Eq. (19). Next, substituting them into Eqs. (7) and (9), to express the energies via the nodal values. After that, substituting the energies into Eq. (10) leads to the equilibrium equations as

$$\left(\mathbf{K}_{\Omega_c}^{L}+\mathbf{K}_{\Omega_c}^{NL}\right)\mathbf{U}_s=\mathbf{Q}_{\Omega_c} \tag{21}$$

In Eq. (21), $\mathbf{K}_{\Omega_c}^{L}$ is the linear stiffness matrix which refers to the matrix of elastic stiffness coefficients $\mathbf{D}_{E1}$; $\mathbf{K}_{\Omega_c}^{NL}$ is the geometric stiffness matrix which refers to the matrices of stiffness coefficients $\mathbf{D}_{E2}$, $\mathbf{D}_{E3}$ and $\mathbf{D}_{E4}$; $\mathbf{Q}_{\Omega_c}$ is the nodal load vector; $\mathbf{U}_s$ is the vector of the nodal values. They are defined by

$$\mathbf{K}_{\Omega_c}^{L}=\int_{\Omega_c}\mathbf{\Lambda}^{\mathrm{T}}\mathbf{D}_{E1}\mathbf{\Lambda}d\Omega_c \tag{22}$$

$$\mathbf{K}_{\Omega_c}^{NL}=\int_{\Omega_c}\left(\frac{\partial\mathbf{H}^{\mathrm{T}}}{\partial x}\mathbf{D}_{E2}\mathbf{\Lambda}+\frac{\partial\mathbf{H}^{\mathrm{T}}}{\partial x}\mathbf{D}_{E3}\frac{\partial\mathbf{H}}{\partial x}+\mathbf{\Lambda}^{\mathrm{T}}\mathbf{D}_{E4}\frac{\partial\mathbf{H}}{\partial x}\right)d\Omega_c \tag{23}$$

$$\mathbf{Q}_{\Omega_c}=\int_{\Omega_c}bq_o\mathbf{H}^{\mathrm{T}}d\Omega_c \tag{24}$$

$$\begin{cases}\mathbf{U}_s=\left\{...u_{om},\hat{u}_{om},w_{om},\hat{w}_{om},\theta_{om},\hat{\theta}_{om}...\right\}^{\mathrm{T}}\\ m=1,2,...,\text{total number of nodes in }\Omega_s\end{cases} \tag{25}$$

In Eq. (25), $(\circ)_{om}$ and $(\hat{\circ})_{om}$ represent for the function values of function $(\circ)$ and its first derivative at the coordinate of the m-th node, respectively.

The matrix $\mathbf{\Lambda}$ and vector $\mathbf{H}$ in Eqs. (22-24) are determined via the shape functions $\psi(x)$ and $\psi_\varphi(x)$ (extracting from Eq. (20)) as follows

$$\mathbf{\Lambda}=\begin{bmatrix}... & \frac{\partial\psi^{(m)}}{\partial x} & \frac{\partial\psi_\varphi^{(m)}}{\partial x} & 0 & 0 & 0 & 0 & ...\\ ... & 0 & 0 & \frac{\partial^2\psi^{(m)}}{\partial x^2} & \frac{\partial^2\psi_\varphi^{(m)}}{\partial x^2} & 0 & 0 & ...\\ ... & 0 & 0 & 0 & 0 & \frac{\partial\psi^{(m)}}{\partial x} & \frac{\partial\psi_\varphi^{(m)}}{\partial x} & ...\\ ... & 0 & 0 & 0 & 0 & \psi^{(m)} & \psi_\varphi^{(m)} & ...\end{bmatrix}_{4\times 6N} \tag{26}$$

$$\mathbf{H}=\left\{...\quad 0\quad 0\quad \psi^{(m)}\quad \psi_\varphi^{(m)}\quad 0\quad 0\quad ...\right\}_{1\times 6N} \tag{27}$$

For all background cells, Eq. (21) is subsequently assembled into the system of global discrete equations:

$$\left(\mathbf{K}^{L}+\mathbf{K}^{NL}\right)\mathbf{U}=\mathbf{Q}_F \tag{28}$$

where $\mathbf{K}^L$ and $\mathbf{K}^{NL}$ are the global stiffness matrices, $\mathbf{Q}_F$ is the global load vector, and $\mathbf{U}$ is the global nodal value vector.

It should be noted that the linear analysis is recovered by neglecting the matrix $\mathbf{K}^{NL}$ in Eq. (28).

3. Numerical examples and discussion

In this section, two types of axially immovable edge conditions are considered. They are fully clamped and hinged edges which are, respectively, abbreviated as C and H in the presentation. Their kinematic conditions require as

$$\text{Clamped (C):}\quad u_o=w_o=\frac{\partial w_o}{\partial x}=\theta_o=0 \tag{29}$$

$$\text{Hinged (H):}\quad u_o=w_o=0 \tag{30}$$

In mesh-free modeling, the size of the influence domain is designed to collect 3-4 nodes per domain, and uniformly distributed nodes are used.

Because the geometric stiffness matrix depends on the nodal displacements, i.e., $\mathbf{K}^{NL}=\mathbf{K}^{NL}(\mathbf{U})$, Eq. (28) is a nonlinear equation and has to be solved by iterative methods. In this work, the direct iterative method is employed. The solution of Eq. (28) for the n-th iteration can be stated as

$$\left[\mathbf{K}^{L}+\mathbf{K}^{NL}\left(\mathbf{U}^{(n-1)}\right)\right]\mathbf{U}^{(n)}=\mathbf{Q}_F \tag{31}$$

The iteration is supposed to achieve convergence if the solution satisfies the following condition

$$\sqrt{\frac{\mathbf{\Delta U}\cdot\mathbf{\Delta U}}{\mathbf{U}^{(n)}\cdot\mathbf{U}^{(n)}}}\le 1\mathrm{e}^{-3},\ \mathbf{\Delta U}=\mathbf{U}^{(n)}-\mathbf{U}^{(n-1)} \tag{32}$$

To accelerate the convergence, a weighted average of the solutions, i.e., $\overline{\mathbf{U}}^{(n-1)}$, instead of $\mathbf{U}^{(n-1)}$, proposed by Reddy [19], is employed to evaluate the matrix $\mathbf{K}^{NL}$ at the n-th iteration.

$$\overline{\mathbf{U}}^{(n-1)}=\beta\mathbf{U}^{(n-2)}+(1-\beta)\mathbf{U}^{(n-1)} \tag{33}$$

where β is the parameter tested to avoid the non-convergence in the analysis. In this study, β = 0.25 is selected and numerical analyses show that it results in stable convergence.

3.1. Convergence test and validation

To test the convergence of the mesh-free analysis, raising the number of distributed nodes (mesh level) in the influence domain until the results of the two adjacent analyses are almost the same. The test is done for linear bending of single layer FGM beam by ignoring the porous core and the bottom skin. The function of Young's modulus is given by

$$E=E_c+(E_m-E_c)\left(\frac{z}{h}+\frac{1}{2}\right)^k \tag{34}$$

Geometry sizes of the beam and material properties of the FGM are L = 1 m, $b=h=1\times10^{-2}$ m, E_m = 200 GPa, E_c = 20 GPa, $\nu_m=\nu_c$ = 0.25. The FGM beam is subjected to uniformly distributed load q_o or sinusoidally distributed load

$q_o\sin(\pi x/L)$, q_o = 2.5 N/m. This beam with CC edges was conducted by Wang et al. [11] via the Ritz method and Reddy et al. [16] via the finite element method. The obtained results are reported in Table 1. Very good convergence is achieved, and the mesh levels with 31 and 41 nodes yield almost the same results. Thus, the 31-node mesh level will be used in the next investigations. Besides, the studied results match well with those of Wang et al. [11] and Reddy et al. [16].

Next, the validation is performed for the nonlinear flexural bending of the sandwich porous beam with isotropic skins under a distributed load of q_o = 50 kN/m. Geometry parameters and material properties are L = 1 m, $b = h = 5\times10^{-2}$ m, E_m = 200 GPa, ν_m = 0.3. This problem was studied by Wang et al. [11] and Srikarun et al. [13]. For comparison purposes, replacing $E(z)$ by $E(z)/(1-\nu^2)$ in Eq. (5) and setting k = 0 in Eq. (1) to be compatible with the studies of Wang and co-workers [11] and Srikarun and co-workers [13]. Non-dimensional mid-span deflection $\hat{w} = w(L/2)/h$ of the beam with HH edges is illustrated in Table 2. Again, a good agreement can be seen, which confirms the validation.

3.2. Comprehensive study

In this part, the effects of important parameters on linear and nonlinear bending of PFGM sandwich beams are performed to comprehend their characteristics. It is assumed that (a) FGM of the skins is composed of ceramic (E_c = 380 MPa, ν_c = 0.3) and metal (E_m = 70 MPa, ν_m = 0.3) [2]; (b) the porous core is a metal foam (E_m = 70 MPa, ν_m = 0.3) [2]. The geometrical parameters of the sandwich beam are L = 1 m, h/b = 1. Non-dimensional deflection $\hat{w} = w/h$ is used for the presentation.

Table 1. *Convergence and comparison of central deflection w(L/2) (unit: 10^{-5} m) of single layer FGM beam (linear analysis)*

Number of nodes	For uniformly distributed load		For sinusoidally distributed load	
	k = 0.0	k = 1.0	k = 0.0	k = 1.0
5	3.91072	9.15041	3.30830	7.74097
11	3.91083	9.15062	3.30838	7.74107
21	3.91088	9.15071	3.30841	7.74113
31	3.91090	9.15074	3.30842	7.74115
41	3.91092	9.15078	3.30844	7.74118
Ref. [11]	3.91075	9.15046	3.30832	7.74097
Ref. [16]	3.9109	9.1508	3.3079	7.7400

Table 2. *Validation of the deflection $\hat{w}(L/2)$ of sandwich beam with porous core (nonlinear analysis, h_c/h_f = 8)*

e_o	This study	Ref. [11]	Ref. [13]
0	0.110417 (5)*	0.110413	0.108052
0.25	0.115868 (5)*	0.115864	0.113392
0.5	0.122006 (5)*	0.122001	0.119408
0.75	0.129072 (5)*	0.129067	0.126338

(•) implies the number of iterations satisfying the convergence of Eq. (32).*

Effects of porosity coefficient (e_o), power-law index (k), core-to-skin thickness ratio (h_c/h_f) and edge conditions on the non-dimensional central deflection of PFGM sandwich beams under uniformly distributed load (q_o) with different levels are depicted in Figure 2 - Figure 5, respectively. The beam with length-to-height ratio L/h = 50 is selected for these investigations.

Meticulously observing Figure 2-Figure 5 shows that (a) when applied load q_o increases, the deflection varies linearly if the effect of geometric nonlinearity is not considered. On the contrary, it varies nonlinearly if this effect is included; (b) at the same load level, nonlinear deflection is smaller than linear one. This is due to the additional matrix $\mathbf{K}^{NL}$ of the nonlinear analysis making the system stiffer in the current study. In other words, the stiffness of the beam can increase if it is included the effect of nonlinear deformation. In addition, the greater the applied load is, the greater the discrepancy between linear and nonlinear deflections is. Thus, neglecting the geometric nonlinearity may result in significantly overestimated deflection of the beam under a large applied load; (c) effects of k, h_c/h_f, and edge conditions on the linear deflection are much stronger than the nonlinear one. The gaps between the plots of the linear deflection increase with increasing applied load q_o, whereas those of the nonlinear deflection have small changes.

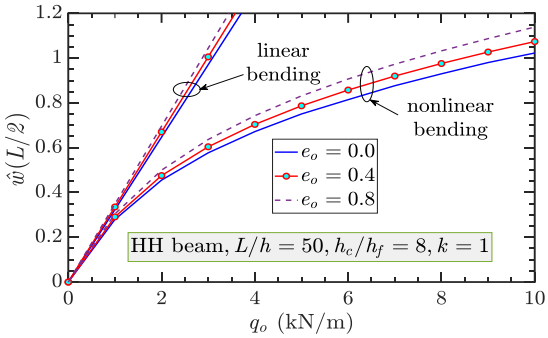

Figure 2. *Effects of e_o on the deflection $\hat{w}(L/2)$ of PFGM sandwich beam*

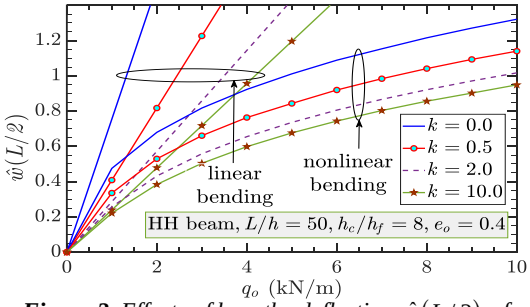

Figure 3. *Effects of k on the deflection $\hat{w}(L/2)$ of PFGM sandwich beam*

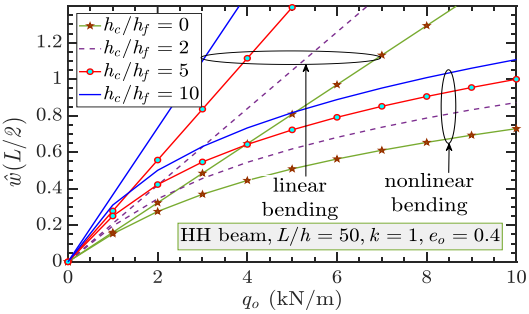

Figure 4. *Effects of h_c/h_f on the deflection $\hat{w}(L/2)$ of PFGM sandwich beam*

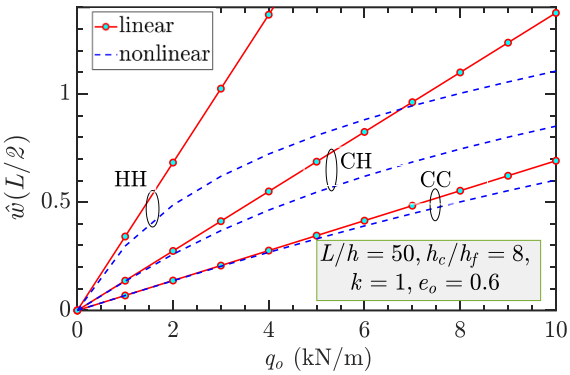

Figure 5. *Effects of edge supports on the deflection* $\hat{w}(L/2)$ *of PFGM sandwich beam*

Figure 2 shows that the deflection increases with increasing e_o. This is because the beam with higher of pore density (higher value of e_o) is softer. In contrast, as shown in Figure 3, the deflection decreases when k increases. This is because increasing the value of k leads to an increase in the ceramic constituent which has a greater Young's modulus. In other words, the beam becomes stiffer as k increases or e_o decreases.

It is clear in Figure 4 that the PFGM sandwich beam becomes weaker if the thickness of the core is greater (higher h_c/h_f). Consequently, it gives a greater deflection.

Finally, among the three edge types of the beam as illustrated in Figure 5, the HH beam gives the greatest deflection, whereas the smallest one belongs to the CC beam. It is also interesting that when applied load q_o increases, the geometric nonlinearity has the strongest impact on the HH beam, but the smallest one on the CC one.

4. Conclusions

Linear and nonlinear static deflections of sandwich beam with a porous core and two skins made of FGM are investigated. Material properties of the beams are tailored so they are continuous along the thickness direction. The equilibrium equation including the von Kármán geometric nonlinearity is derived from the virtual work principle in conjunction with TOBT. The C^1 Hermite interpolation based-mesh-free approach is utilized to discretize the equilibrium equation. The direct iterative method with the weighted average of the solutions is adopted to deal with the nonlinear system of equations. The study shows the efficiency of the mesh-free approach with a high convergence rate. The correctness and reliability of the developed formulations are confirmed. The numerical results show the significantly overestimated deflection of the beam under a large applied load if the geometric nonlinearity is neglected in the analysis. Furthermore, the power-law index, porosity coefficient, core-to-skin thickness ratio, and edge conditions have important effects on the linear and nonlinear deflections of the studied beams.

Acknowledgment: This work was supported by The University of Danang - University of Science and Technology, code number of Project: B2022-DN02-08.

REFERENCES

[1] L. Mu and G. Zhao, "Fundamental Frequency Analysis of Sandwich Beams with Functionally Graded Face and Metallic Foam Core", *Shock and Vibration*, vol. 2016, p. 3287645, 2016.

[2] Y. Wang, A. Zhou, T. Fu, and W. Zhang, "Transient response of a sandwich beam with functionally graded porous core traversed by a non-uniformly distributed moving mass", *International Journal of Mechanics and Materials in Design*, vol. 16, no. 3, pp. 519-540, 2020.

[3] T. H. Chinh, T. M. Tu, D. M. Duc, and T. Q. Hung, "Static flexural analysis of sandwich beam with functionally graded face sheets and porous core via point interpolation meshfree method based on polynomial basic function", *Archive of Applied Mechanics*,vol. 91, pp. 933-947, 2021.

[4] D. X. Hung and H. Q. Truong, "Free vibration analysis of sandwich beams with FG porous core and FGM faces resting on Winkler elastic foundation by various shear deformation theories", *Journal of Science Technology in Civil Engineering NUCE*, vol. 12, no. 3 pp. 23-33, 2018,.

[5] T. Q. Hung and T. M. Tu, "Free vibration of piezoelectric FGM sandwich beam with porous core embedded in thermal environment and elastic foundation", *Journal of Science and Technology in Civil Engineering (STCE)-HUCE*, vol. 15, no. 4, pp. 15-28, 2021.

[6] T. Q. Hung, D. M. Duc, and T. M. Tu, "Static Behavior of Functionally Graded Sandwich Beam with Fluid-Infiltrated Porous Core", in *Modern Mechanics and Applications*: Springer, 2022, pp. 691-706.

[7] M. Derikvand, F. Farhatnia, and D. H. Hodges, "Functionally graded thick sandwich beams with porous core: Buckling analysis via differential transform method", *Mechanics Based Design of Structures Machines*, vol. 51, no. 7, pp. 3650-3677, 2021.

[8] N. D. Duc, K. Seung-Eock, N. D. Khoa, and D. Q. Chan, "Nonlinear buckling and post-buckling analysis of shear deformable stiffened truncated conical sandwich shells with functionally graded face sheets and a functionally graded porous core", *Journal of Sandwich Structures & Materials*, Vol. 23, no. 7, 2020.

[9] N. V. Nguyen, H. Nguyen-Xuan, and J. Lee, "A quasi-three-dimensional isogeometric model for porous sandwich functionally graded plates reinforced with graphene nanoplatelets", *Journal of Sandwich Structures & Materials*, Vol. 24, no. 2, 2021.

[10] J. Lin, J. Li, Y. Guan, G. Zhao, H. Naceur, and D. Coutellier, "Geometrically nonlinear bending analysis of functionally graded beam with variable thickness by a meshless method", *Composite Structures*, vol. 189, pp. 239-246, 2018.

[11] Y. Wang, H. Ma, K. Xie, T. Fu, J. Chen, and Y. Liu, "Nonlinear bending of a sandwich beam with metal foam and GPLRC face-sheets using Chebyshev–Ritz method: Effects of agglomeration and internal pore", *Thin-Walled Structures*, vol. 181, 110035, 2022.

[12] S. J. Salami, "Large deflection geometrically nonlinear bending of sandwich beams with flexible core and nanocomposite face sheets reinforced by nonuniformly distributed graphene platelets", *Journal of Sandwich Structures and Materials*, vol. 22, no. 3, pp. 866-895, 2020.

[13] B. Srikarun, W. Songsuwan, and N. Wattanasakulpong, "Linear and nonlinear static bending of sandwich beams with functionally graded porous core under different distributed loads", *Composite Structures*, vol. 276, pp. 114538, 2021.

[14] C. Feng, S. Kitipornchai, and J. Yang, "Nonlinear bending of polymer nanocomposite beams reinforced with non-uniformly distributed graphene platelets (GPLs)", *Composites Part B: Engineering*, vol. 110, pp. 132-140, 2017.

[15] L. Li, X. Li, and Y. Hu, "Nonlinear bending of a two-dimensionally functionally graded beam", *Composite Structures*, vol. 184, pp. 1049-1061, 2018.

[16] J. N. Reddy, S. El-Borgi, and J. Romanoff, "Non-linear analysis of functionally graded microbeams using Eringen′ s non-local differential model", *International Journal of Non-Linear Mechanics*, vol. 67, pp. 308-318, 2014.

[17] D.-G. Zhang, "Nonlinear bending analysis of FGM beams based on physical neutral surface and high order shear deformation theory", *Composite Structures*, vol. 100, pp. 121-126, 2013.

[18] T. Q. Hung, D. M. Duc, and T. Minh Tu, "Static bending mesh-free analysis of smart piezoelectric porous beam reinforced with graphene platelets", *Proceedings of the Institution of Mechanical Engineers, Part C: Journal of Mechanical Engineering Science*, Vol. 237, no. 7, 2022.

[19] J. N. Reddy, *An Introduction to Nonlinear Finite Element Analysis Second Edition: with applications to heat transfer, fluid mechanics, and solid mechanics.* OUP Oxford, 2014.